David Tomás Sánchez Martínez
Lourdes García Rodríguez
(coordinadores)

Proceedings of the 7th International Seminar on ORC Power Systems

Editorial Universidad de Sevilla

Proceedings of the 7th International Seminar on

ORC
Power Systems

David Tomás Sánchez Martínez
Lourdes García Rodríguez
(coordinadores)

Proceedings of the 7th International Seminar on

ORC Power Systems

(ORC2023)

4th to 6th
SEPTEMBER
SEVILLE 2023

EUS EDITORIAL UNIVERSIDAD DE SEVILLA

Sevilla, 2024

Colección Actas
Núm.: 91

Review chairs of the 7th International Seminar on ORC Power Systems

Prof. Christoph Wieland (University of Duisburg-Essen) - *Review Chair*
Prof. Sotirios Karellas (National Technical University of Athens) - *Review Co-Chair*
Prof. Teemu Turunen-Saaresti (LUT University) - *Review Co-Chair*
Dr. Diego-César Alarcón-Padilla (Plataforma Solar de Almería - CIEMAT) - *Review Co-Chair*
Dr. Francesco Crespi (Universidad de Sevilla) - *Review Co-Chair*

ISBN 978-84-472-2745-7
DOI: https://dx.doi.org/10.12795/9788447227457

Diseño de cubierta y maquetación: los autores

INDEX OF CONTRIBUTIONS

DOI: https://dx.doi.org/10.12795/9788447227457_59

Numerical Analysis of Aerodynamics and Performance of a Radial-Inflow Micro-ORC Turbine

Fatemeh Ardaneh[1,2*], Marta Zocca[1], Antti Uusitalo[1], Teemu Turunen-Saaresti[1]

[1] *LUT University, School of Energy Systems, P.O. Box 20, 53851 Lappeenranta, Finland*
[2] *Turku University of Applied Sciences, Computational Engineering and Analysis Research Group, Engineering and Business, Technology Industry, Joukahaisenkatu 3, 20520 Turku, Finland*

* Corresponding Author: Fatemeh.Ardaneh@lut.fi

ABSTRACT

Organic Rankine Cycle (ORC) has proven to be an effective way to recover waste heat. The performance of ORC systems is profoundly affected by turbine selection, which is one of the most critical components. In this study, a numerical aerodynamic analysis of a micro-ORC turbine is carried out as an effort towards the formulation of a reduced order model (ROM) of the turbine for the dynamic simulation of the complete ORC system. The studied turbine is the radial-inflow turbine of the waste heat recovery micro-ORC test rig at the Laboratory of Fluid Dynamics, LUT University. The performance of the turbine, which features a highly supersonic flow at the stator outlet, is evaluated through steady-state CFD simulations of the complete turbine geometry using linear siloxane MDM (Octamethyltrisiloxane $C_8H_{24}O_2Si_3$) as working fluid. Results are discussed and compared with experimental data. Turbine efficiency is studied numerically at varying rotational speeds (25000-31000 rpm). A significant fluctuation in the flow angle at the stator is observed at low rotational speeds, while it decreases at higher speeds. At increasing rotational speed, the analysis shows a corresponding increase in the discharged flow rate, and the turbine efficiency up to 0.2061 kg/s and 79.3, respectively. Moreover, the flow features through the turbine nozzle ring and rotor blades are examined and discussed for selected operating conditions.

1. INTRODUCTION

Organic Rankine cycle (ORC) power systems with low capacity and high temperature are increasingly investigated due to the potential for large markets for distributed renewable energy conversions and mobile/stationary heat recovery (Colonna et al., 2015). As rotary volumetric machines are limited in their maximum pressure ratio, a kinetic type of turbines are often favored for reaching high conversion efficiency and high expansion ratios, that are required especially in high temperature ORC applications (Zhao et al., 2019). Radial-inflow turbine can be considered as a feasible choice because of its compactness, high power density, and high flow coefficient. High expansion efficiency, on the other hand, is particularly challenging (De Servi et al., 2019). In order to achieve high expansion efficiency, machines must have a supersonic radial stator and a normal radial-inflow rotor, both of which are difficult to design because of their small size and significant real gas effects along the expansion (Colonna et al., 2006).

Both numerical and experimental methods have been used in various publications to investigate ORC turbine geometry, performance, real gas effects, and flow characteristics. Design and experimental study of ORC and radial turbines to improve efficiency are always an interesting subject for researchers. The study by Weiß et al. (2018) examined two micro-turbines for small ORC plants, an axial impulse turbine and a radial cantilever. This study shows that these turbines are efficient expanders for ORC plants. However, the radial cantilever is generally more efficient than the axial impulse equivalent. Also, the working fluid selection greatly affects the thermodynamics, performance, and size of the ORC machinery (Wang et al., 2011). The design and performance prediction of supersonic radial vanes that are used in small-scale ORC turbines for high temperatures was conducted using numerical methods in recent works related to high-temperature small-scale radial-inflow ORC turbines (Li et al., 2022). A CFD simulation by Fiaschi et al. (2016), was used to develop the geometry design of radial ORC expanders from a 0D into a 3D design. In this study, the results of these two approaches were found to be in agreement.

Based on the literature review of radial-inflow micro-ORC turbines, most of the research efforts have been concentrated on designing the turbine and finding more efficient working fluids. There is a lack of discussion and analysis of detailed turbine flow characteristics, mainly, flow angle fluctuations, in both components (rotor and stator). It is also less discussed when it comes to loss issues. Regarding these discussions, there are only a few studies where small-scale and high-expansion-ratio ORC turbines are investigated experimentally. This study addresses this opening issue for the radial-inflow turbine of the waste heat recovery micro-ORC test rig at the Laboratory of Fluid Dynamics, LUT University. This study compares experimental results with steady-state numerical simulations of the introduced turbine. The investigated conditions were selected based on the available experimental data with four different rotational speeds. In addition, the simulations are carried out at the turbine design condition. The difference between numerical and experimental data is investigated with focus on the details of the flow characteristics at different rotational speeds (and pressure ratio) and their effect on the performance of the micro-ORC turbine. The micro-ORC test facility utilizes high-temperature exhaust gas heat of the diesel generator and the working fluid is siloxane MDM (Octamethyltrisiloxane $C_8H_{24}O_2Si_3$) (Turunen-Saaresti et al., 2017).

It should be noted that previous research has been done already with the experimental setup in recent years. By analyzing the preliminary radial turbine design calculations, Uusitalo et al. (2013) found that larger turbine wheels with higher outlet blade heights and lower rotational speed can be designed with molecularly complex fluids, which can be beneficial for small-scale ORC units. Uusitalo et al. (2014) designed a small-scale ORC turbine stator for the experimental radial turbine. This supersonic design took into account flow characteristics and shock waves through convergent-divergent nozzles. In addition, a CFD analysis on the magnitude of expansion losses and their effect on the performance of radial turbines is presented by Uusitalo and Zocca (2023). 364

2. METHODOLOGY

The experimental setup and CFD model are introduced. Also, the case study is presented to discuss the reason for choosing the numerical model presented in the result section. In the current work, the average of the experimental data at each rotational speed is calculated and compared with the steady-state numerical simulations. To compare in detail, the results of pressure, Mach number, relative velocity, and flow angle are investigated for both stator and rotor components. The investigated flow angles are the angle of absolute and relative velocity, shown in Figure 1.

2.1 Description of the experimental setup

The experimental data have been obtained from the micro-ORC test setup at LUT. The experimental ORC system recovers high temperature exhaust gas heat from a 150-200 kW scale diesel engine. The ORC is equipped with a supersonic radial turbine, permanent magnet generator, and a partial admission type of feed pump assembled on the same shaft with a nominal rotational speed of 31 000 rpm. The turbogenerator is hermetically sealed and the bearings are lubricated by using liquid MDM. The low pressure working fluid vapor is used for generator cooling. In the experiments, the rotational speed of the turbogenerator can be controlled via a frequency converter, which allows to adjust the turbine operation at different off-design conditions. It is worth noting that as the main feed pump of the system is assembled on the turbogenerator shaft, the rotational speed directly affects the turbine inlet pressure and working fluid mass flow rate. Several test runs have been carried out with the experimental system and the performance of the turbine has been investigated under conditions which are close to the system design conditions. In addition, the operation has been experimentally investigated at several off-design

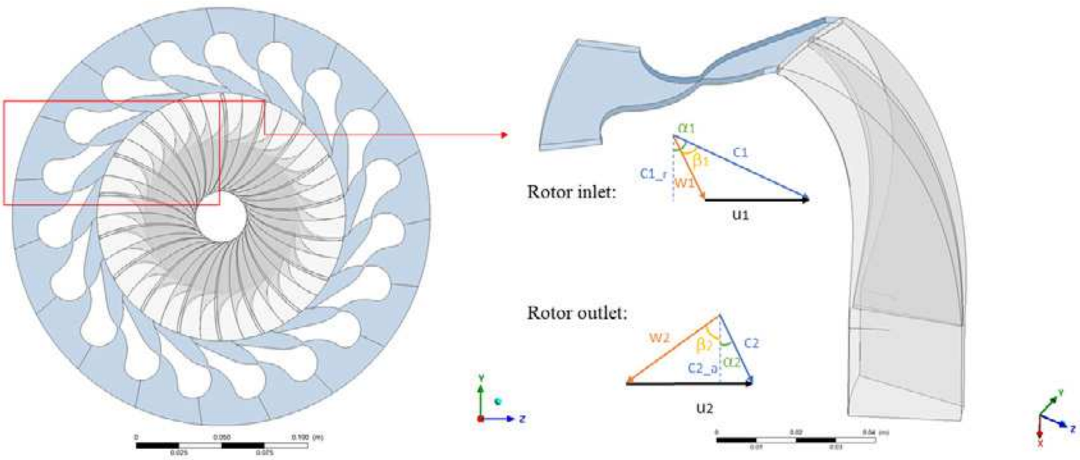

Figure 1: Top view of the LUT micro-ORC turbine (left). Geometry of the computational domain (one passage) and velocity triangles at rotor inlet and outlet (right).

Table 1: Design conditions of the LUT micro-ORC turbine (left). Reference turbine operating conditions from experimental runs (right). The conditions at 31 000 rpm are the design point.

Turbine power	12 kW
Turbine efficiency	76 %
Fluid mass flow rate	0.2 kg/s
Rotor diameter	144 mm
Blade height at the rotor inlet	2 mm
Mach number at the stator outlet	2.2
Specific speed, Flow coefficient	0.5, 0.4

N [rpm]	T1 [^{o}C]	p1 [bar]	T2 [^{o}C]	p2 [bar]
25298	252.3	6.515	219.9	0.094
27057	252.8	6.653	216.6	0.099
28835	255	6.713	219.2	0.098
30623	251.2	6.879	213	0.098
31000	***265***	***7.900***	-	***0.070***

points. The turbine measurements include the pressure and temperature measurements at the inlet and outlet, as well as mass flow measurement. The fluid thermodynamic properties, such as density and enthalpy have been defined by using the measured temperature and pressure data. The mass flow rate of MDM has been measured by using an oval gear meter, measuring the liquid working fluid flow rate entering the evaporator. The main design parameters of the investigated turbine and measured operation conditions are presented in Table 1. The experimental setup, experimental results and measurement uncertainties are discussed and analyzed in detail in Uusitalo et al. (2020).

Figure 2: Numerical grid

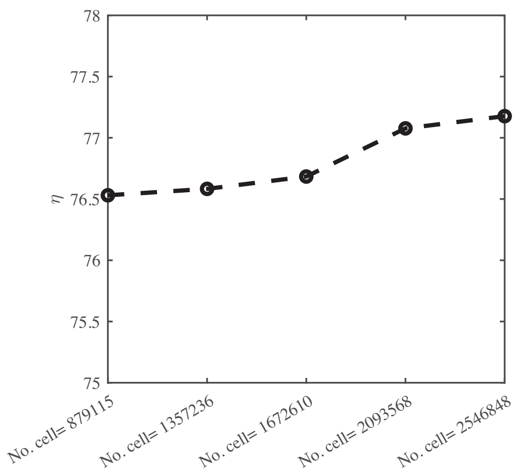

Figure 3: Grid independence study based on the turbine efficiency.

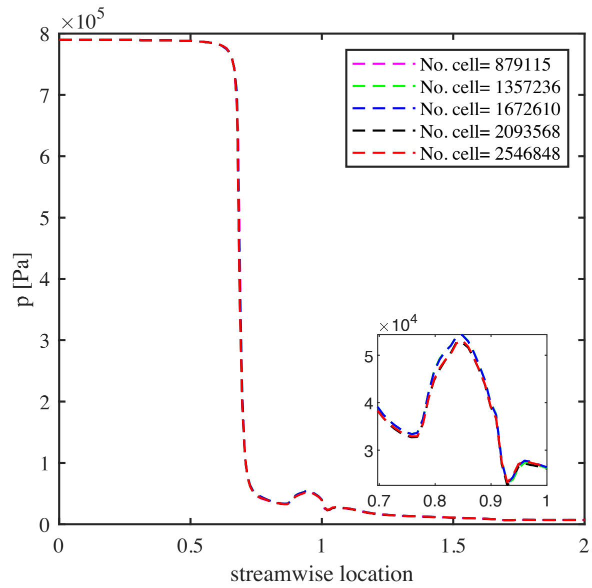

Figure 4: Grid independence study based on the area average of static pressure from inlet to outlet of the turbine. Streamwise locations 0-1 represent the stator. Streamwise locations 1-2 represent the rotor.

2.2 Computational Fluid Dynamic analysis methods

Simulations were performed using Ansys CFX, and structured grids were generated using Pointwise. An exemplary grid is shown in Figure 2. A finite-volume-based method for the solution of the RANS equations using the k–ω SST turbulence model (Menter, 1993; Menter et al., 2003) is used in steady-state simulations. Simulations were conducted using a stator flow channel and a rotor flow channel modeled with periodic boundary conditions, representing blade row periodicity. Both the frozen-rotor and the mixing-plane approaches (ANSYS, 2019) were used to model the interface between the stator and the rotor, namely the non-rotating domain and the rotating domain. As the boundary conditions for the simulations, temperature and pressure were set as the inlet conditions, and the outlet boundary condition was static pressure. The boundary conditions applied in the CFD simulations are reported in Table 1 for all the studied operating points. Convergence residuals and simulated mass imbalance were used to monitor the convergence of the simulations.

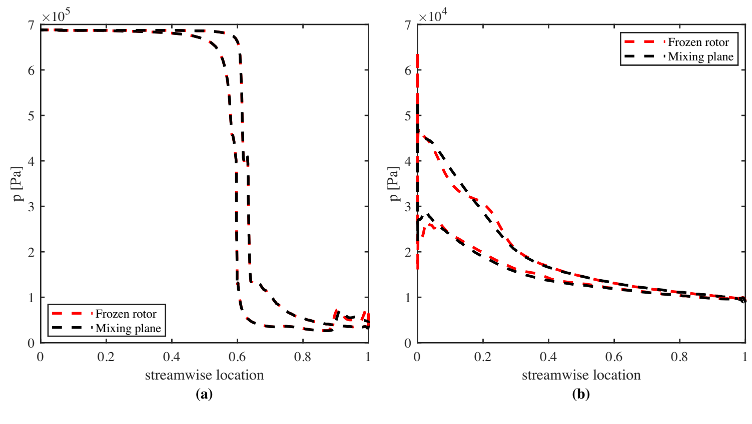

Figure 5: Comparison of frozen rotor and mixing plane model. Turbine blade loading (Span=0.5) at N=30624rpm. (a) Stator, (b) Rotor.

Table 2: Grid independence study. The grid of case 4 is the one used throughout the numerical study.

Case No.	Number of cells	η	Deviation of η with respect to case 4 (%)
1	879115	76.5	0.71
2	1357236	76.5	0.64
3	1672610	76.6	0.51
4	2093568	77.0	-
5	2546848	77.1	-0.13

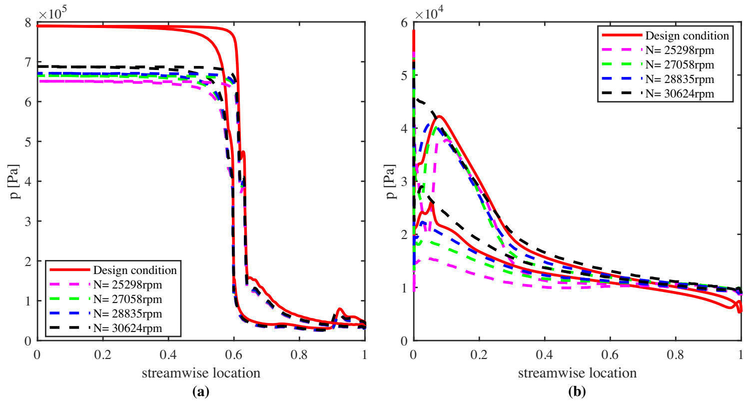

Figure 6: Turbine blade loading (Span=0.5). (a) Stator, (b) Rotor

A grid independence study was performed for the turbine in design conditions using the frozen rotor model and five grid resolutions. Results are presented in Figure 3, 4 and in Table 2. Generally, the results of all cases are similar with high accuracy, but the most significant differences in the flow structure are occurring at the stator trailing edge, where shock waves are present. As it can be seen from Figure 4, such differences are observed up to the grid resolution of case 4, since results of case 4 and 5 overlap. The grid resolution of case 4 with fewer cells is selected for the rest of the simulations. The overall efficiency of the turbine obtained in each case is presented in Table 2. CFD simulations are performed using both the frozen rotor and the mixing plane models in the stator-rotor interface in order to compare the results between these two approaches. In this section, an example of the results of these models at rotational speed equal to 30624 rpm is presented. Figure 5a-b shows the turbine blade loading on both stator and rotor components. The results of these simulations demonstrate the similarity between the two models. Due to this result, the grid study done with the frozen rotor model can be considered acceptable for the mixing plane model. In addition, it is sufficient to analyze the results of one model. Consequently, the results of section 3 are limited to the mixing plane model.

3. RESULTS AND DISCUSSIONS

The turbine stator and rotor blade loading are presented in Figure 6a-b. Pressure and Mach number from stator inlet to rotor outlet are presented in Figure 7a-b. The trends of pressure and Mach number along the expansion are similar in all the studied operating conditions, as shown in Figures 6 and 7 . The pressure decreases and the Mach number increases rapidly near the throat section of the stator. The most notable differences between the different cases occur near the stator outlet, which is the flow area where shock waves are present. This difference can be observed in the divergent section of the stator nozzle, as shown in Figure 6a. Note that the streamwise location on the figure is the dimensionless distance from the inlet to the outlet. In addition, there are some differences in the rotor pressures and Mach numbers between the cases, as are shown in Figure 6b and 7b. The pressure is lower when rotational speed is lower, however the design rotational speed seems to be exception. It is worth noting that the rotor outlet Mach number is significantly higher in the design condition when compared to the other cases. This is mainly because a lower turbine outlet pressure was used in the turbine design, when compared to the

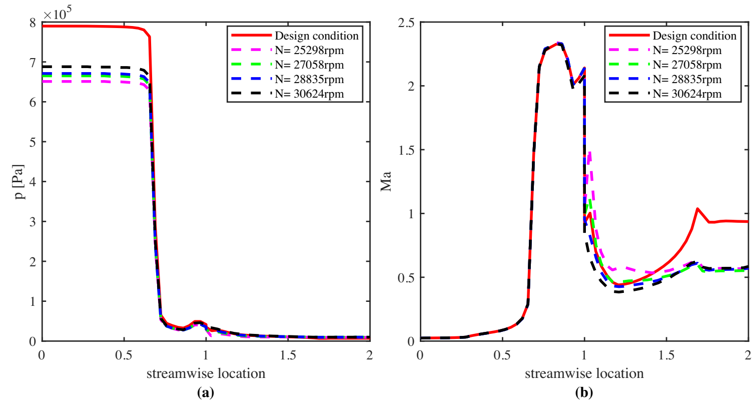

Figure 7: Area average of (a) pressure and (b) Mach number from inlet to outlet of the turbine. Streamwise locations 0-1 represent the stator. Streamwise locations 1-2 represent the rotor.

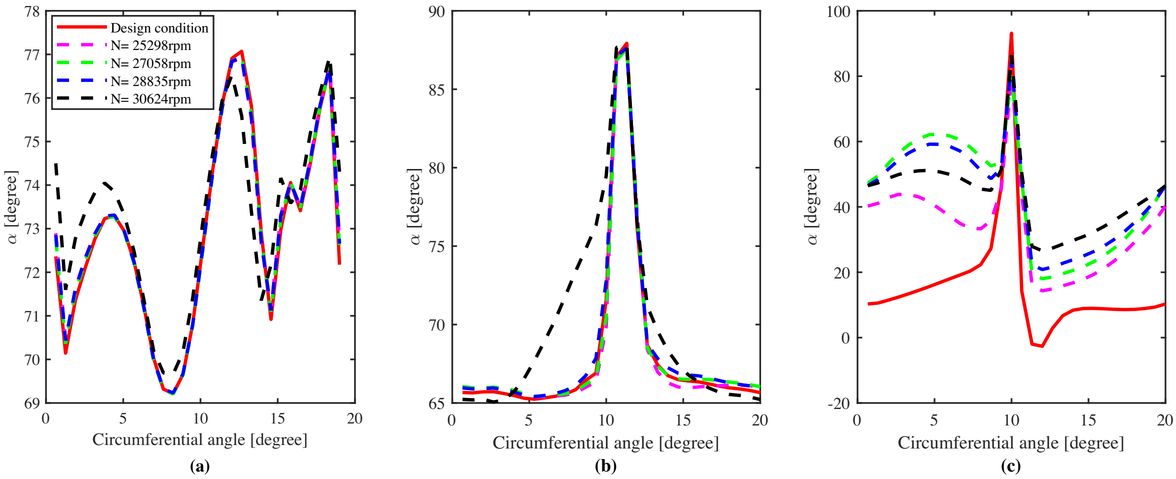

Figure 8: Flow angle distribution at: (a) Stator trailing edge(Span=0.5, streamwise=0.947), (b) Rotor leading edge(Span=0.5, streamwise=1), (c) Rotor trailing edge (Span=0.5, streamwise=1.72).

turbine outlet pressure reached in the experiments. This leads to higher density and lower velocities in the simulation cases that are based on the experimentally defined values. The flow angle at the stator outlet was investigated, and the results are presented in Figure 8a, as it has significant effect on the rotor inlet flow angle which is affected by the shock wave pattern at the stator outlet. There are higher fluctuations of the flow angle at lower rotational speeds with respect to the higher speeds. This non-uniform flow can lead to increased losses in off-design conditions. As it is expected and shown in Figure 8a, based on the non-uniform flow at the stator outlet, shock waves occur before the flow passes through the rotor. Because of the use of the mixing plane approach (ANSYS, 2019), the shock waves are not affecting the flow angle at the rotor inlet and the pattern of rotor inlet flow angle is generally similar for all the cases, as shown in Figure 8b. Table 3 presents the average value of the flow angle at the inlet and outlet of the rotor. From Figure 8c and Table 3, it can be observed that the averaged absolute flow angle of rotor is not significantly changing between the different cases. It can also be observed that the flow angle at rotor discharge is relatively high, which has an impact on the turbine efficiency as fully axial discharge flow typically maximizes the efficiency of a radial turbine. The high flow angle at the rotor discharge is mainly explained by the high turbine outlet pressure, as well as by the changes in the rotational speed. Figure 9a-b display the streamlines coloured by magnitude of relative velocity at the rotor for 25.3 krpm and 30.6 krpm cases. The Mach number distribution is shown for the same

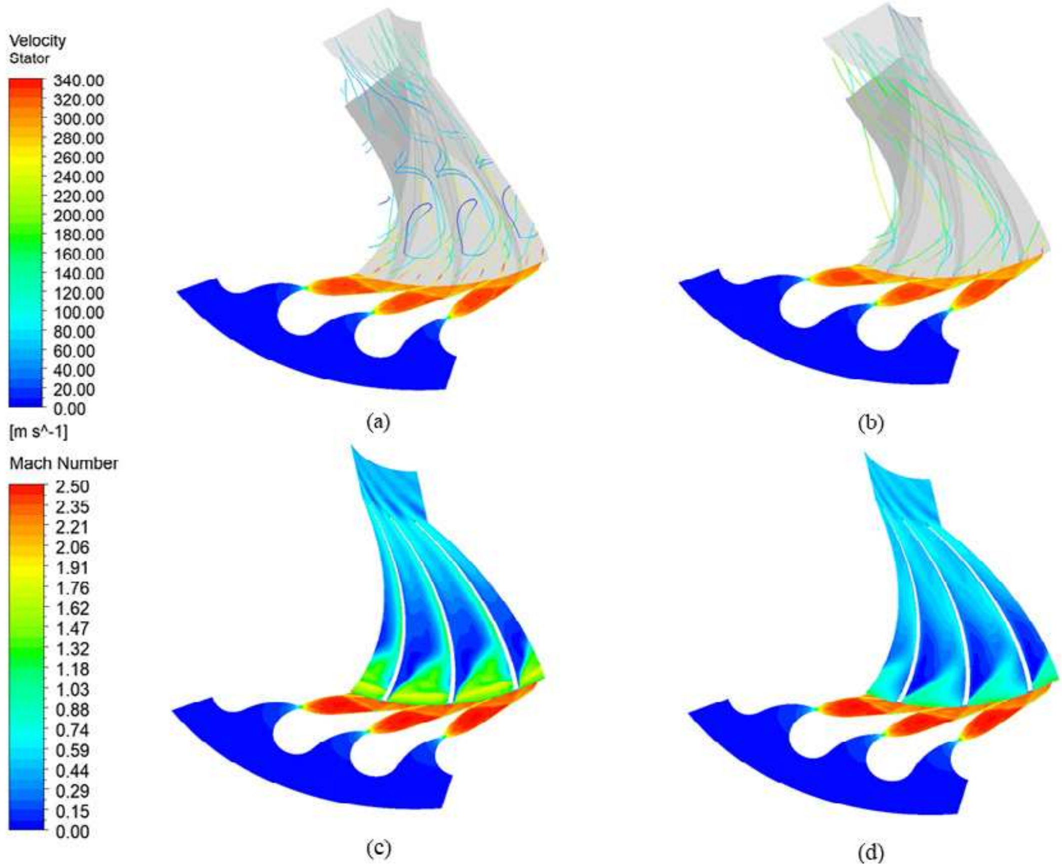

Figure 9: Streamlines coloured by velocity magnitude and Mach number contours in turbine at two different rotational speed: (a) Relative velocity at N=25298rpm, (b) Relative velocity at N=30624rpm, (c) Mach number at N=25298rpm, (d) Mach number at N=30624rpm.

369

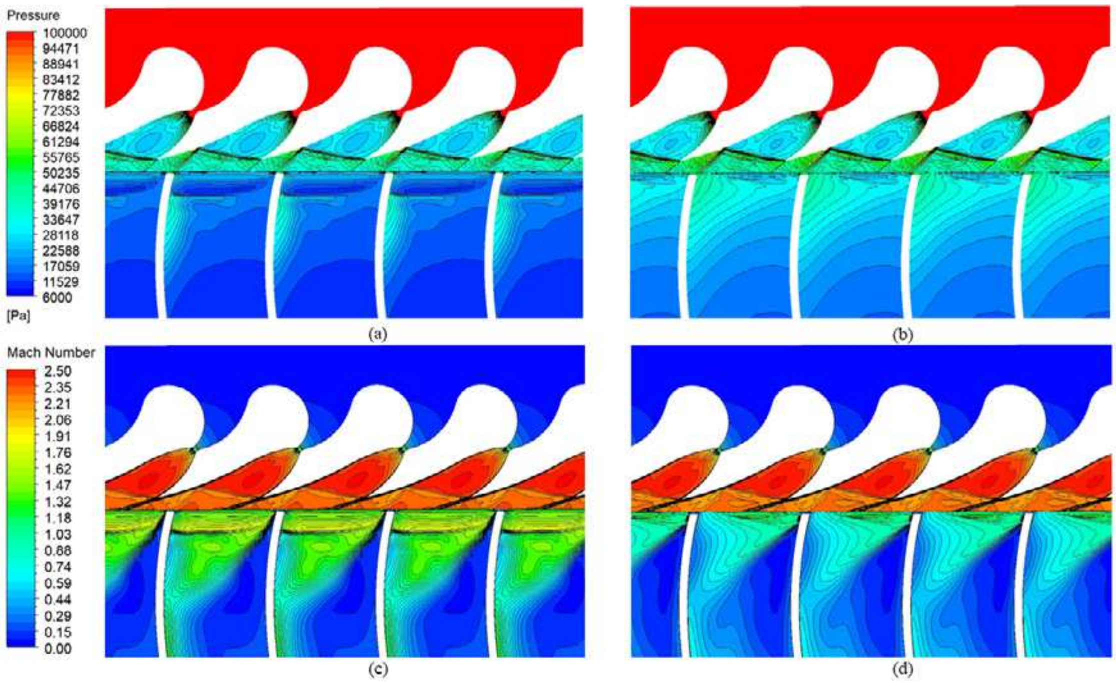

Figure 10: Pressure and Mach number contours in the turbine at two different rotational speeds: (a) Pressure distribution at N=25298rpm, (b) Pressure distribution at N=30624rpm, (c) Mach number at N=25298rpm, (d) Mach number at N=30624rpm.

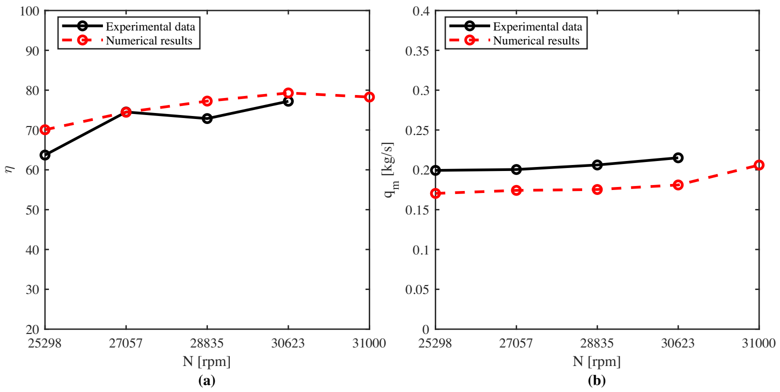

Figure 11: Turbine performance at varying rotational speed: (a) Efficiency, (b) Mass flow rate.

cases in Figure 9c-d. A clear flow separation region can be observed with the case having the lowest rotational speed near the rotor leading edge, whereas a clear flow separation region cannot be observed with the higher rotational speed. This can be explained by the increased incidence with lower rotational speeds, causing flow separation in the rotor and reducing efficiency. A non-uniform flow pattern can be observed in Figure 9c-d at the stator outlet and rotor inlet section caused mainly by the shock waves. More detailed pressure and Mach number distributions at the stator and at the rotor inlet section are shown in Figure 10a-d. Figure 10a-b present the pressure contours in the stator and at the leading edge of the rotor blade. The pressure contours at two different rotational speeds, at the interface between these two components, does not have significant differences. However, in the Mach number contours, the differences between the two cases are more noticeable. The flow is clearly supersonic at the rotor inlet with lower rotational speed and a shock-like pattern is seen, as shown in Figure 10c-d. 370

Table 3: Turbine power and flow angle of absolute velocity at rotor inlet and outlet

N [rpm]	$\alpha 1$ [degree]	$\alpha 2$ [degree]	P [W]
25298	70.9	36.7	7981
27057	70.8	39.7	8582
28835	70.8	40.5	9071
30623	72.1	42.5	9489
31000	***70.6***	***16.5***	***12034***

Table 4: Total efficiency and mass flow rate of the turbine and their difference with respect to the experimental data.

N [rpm]	Exp. η	CFD η	Δ (%)	Exp. q_m	CFD q_m	Δ (%)
25298	63.7	70.0	9.98	0.199	0.170	-14.5
27057	74.5	74.4	-0.08	0.200	0.174	-13.07
28835	72.8	77.2	6.02	0.206	0.175	-14.94
30623	77.2	79.3	2.70	0.215	0.181	-15.85
31000	-	***78.3***	-	-	***0.2061***	-

Figure 11 and Table 4 present the performance of the turbine as resulting from experiments and numerical simulations. The difference of numerical results with respect to the experimental data is also shown in Table 4. Numerical results generally follow the experimentally defined turbine efficiency trend and the efficiency is reduced as the rotational speed is reduced. As it is shown in Figure 11a, there is a decrease in efficiency measured at rotational speed of 28835 rpm while it was not observed in numerical results. It is expected that this is caused by the uncertainty of experimental data. Uncertainties and fluctuations related to the experimental system are discussed more in detail in Uusitalo et al. (2020). Because the temperature drop over the turbine is rather small with MDM, despite the high expansion ratio, even a small deviation in outlet temperature can have a significant effect on the results. Another reason for the difference between the numerical and experimental results is the use of the average of the measurement data at each rotational speed range. The difference between the numerical results and the measurements is more noticeable on the mass flow rate than on the efficiency, as shown in Figure 11b. In addition to measurement uncertainties, the high pressure difference between the inlet and outlet of the stator might lead to some leakage over the stator blade in the experiments, which can partly explain the difference between the measured and simulated mass flows. This is not considered in the numerical simulation, as in the simulations the flow is only going through the stator throat. In the design condition, even though the mass flow rate is higher than the other rotational speeds, the efficiency is lower than at the rotational speed of 30623 rpm. This is mainly due to the fact that at the turbine design conditions, the turbine expansion ratio is greater than in the experimentally investigated operating conditions, which increases the flow velocities and expansion losses, thus reducing efficiency. As the inlet pressure is higher in design conditions, the fluid has higher density at the stator throat, resulting in a higher mass flow rate.

4. CONCLUSIONS

Four different operating conditions were used to evaluate the performance of a radial-inflow micro-ORC turbine using MDM as the working fluid. Numerical simulations were used to analyze the turbine's flow characteristics and performance. The simulation results were compared to experimental measurements. In general, the numerical results and the experimental results have acceptable agreement, predicting similar trends for both the efficiency and the mass flow rate at different operating conditions. At low rotational speeds, significant fluctuations in the flow angle at the stator outlet were observed and a clear flow separation region was predicted to occur in the rotor, due to the high incidence angle at the rotor leading edge. At higher rotational speeds, the mass flow rate, power output and efficiency were increased. In addition, the flow fluctuations at the stator outlet were reduced. It was also observed that the numerical simulations had some deviations in the mass flow rate when compared to measured values. These deviations can be caused for example by leakage flow over the stator blade or by manufacturing tolerances in the stator throat. As a future work, the experimental setup will be updated to provide more detailed measurements of the turbine and to reduce uncertainties related to the measured values. In addition, shock wave stator-rotor interactions could be further investigated with unsteady simulation in the future.

NOMENCLATURE

c	Absolute flow velocity	(m/s)
c_a	Axial component of the absolute velocity	(m/s)
c_r	Radial component of the absolute velocity	(m/s)
Ma	Mach number	(-)
N	Rotational speed	(rpm)
P	Power	(W)
p	Pressure	(Pa, bar)
q_m	Mass flow rate	(kg/s)
T	Temperature	(^{o}C)
w	Relative velocity	(m/s)
α	Flow angle	(degree)
β	Relative flow angle	(degree)
Δ	Deviation with respect to experimental results	(%)
η	Efficiency	(-)
Subscript		
1	Inlet	
2	Outlet	

REFERENCES

ANSYS, I. (2019). Cfx-solver theory guide r19. 2.

Colonna, P., Casati, E., Trapp, C., Mathijssen, T., Larjola, J., Turunen-Saaresti, T., and Uusitalo, A. (2015). Organic Rankine Cycle Power Systems: From the Concept to Current Technology, Applications, and an Outlook to the Future. *Journal of Engineering for Gas Turbines and Power*, 137(10). 100801.

Colonna, P., Nannan, N., Guardone, A., and Lemmon, E. (2006). Multiparameter equations of state for selected siloxanes. *Fluid Phase Equilibria*, 244(2):193–211.

De Servi, C. M., Burigana, M., Pini, M., and Colonna, P. (2019). Design Method and Performance Prediction for Radial-Inflow Turbines of High-Temperature Mini-Organic Rankine Cycle Power Systems. *Journal of Engineering for Gas Turbines and Power*, 141(9). 091021.

Fiaschi, D., Innocenti, G., Manfrida, G., and Maraschiello, F. (2016). Design of micro radial turboexpanders for orc power cycles: From 0d to 3d. *Applied Thermal Engineering*, 99:402–410.

Li, C., Guo, Z., Guo, H., Bao, X., and Zhou, L. (2022). Influences of main design parameters on the aerodynamic performance of a micro-radial inflow turbine. *AIP Advances*, 12(10):105012.

Menter, F. R. (1993). Zonal two equation kw turbulence models for aerodynamic flows. In *23rd fluid dynamics, plasmadynamics*.

Menter, F. R., Kuntz, M., and Langtry, R. (2003). Ten years of industrial experience with the sst turbulence model. *Turbulence, heat and mass transfer*, 4(1):625–632.

Turunen-Saaresti, T., Uusitalo, A., and Honkatukia, J. (2017). Design and testing of high temperature micro-orc test stand using siloxane as working fluid. In *Journal of Physics: Conference Series*, volume 821, page 012024. IOP Publishing.

Uusitalo, A., Turunen-Saaresti, T., Guardone, A., and Grönman, A. (2014). Design and flow analysis of a supersonic small scale orc turbine stator with high molecular complexity working fluid. In *Turbo Expo: Power for Land, Sea, and Air*, volume 45660, page V03BT26A004. American Society of Mechanical Engineers.

Uusitalo, A., Turunen-Saaresti, T., Honkatukia, J., Colonna, P., and Larjola, J. (2013). Siloxanes as Working Fluids for Mini-ORC Systems Based on High-Speed Turbogenerator Technology. *Journal of Engineering for Gas Turbines and Power*, 135(4). 042305.

Uusitalo, A., Turunen-Saaresti, T., Honkatukia, J., and Dhanasegaran, R. (2020). Experimental study of small scale and high expansion ratio orc for recovering high temperature waste heat. *Energy*, 208:118321.

Uusitalo, A. and Zocca, M. (2023). Design and numerical analysis of supersonic radial-inflow turbines for transcritical orc processes. *Energy Conversion and Management*, 277:116609.

Wang, E., Zhang, H., Fan, B., Ouyang, M., Zhao, Y., and Mu, Q. (2011). Study of working fluid selection of organic rankine cycle (orc) for engine waste heat recovery. *Energy*, 36(5):3406–3418.

Weiß, A. P., Popp, T., Müller, J., Hauer, J., Brüggemann, D., and Preißinger, M. (2018). Experimental characterization and comparison of an axial and a cantilever micro-turbine for small-scale organic rankine cycle. *Applied Thermal Engineering*, 140:235–244.

Zhao, Y., Liu, G., Li, L., Yang, Q., Tang, B., and Liu, Y. (2019). Expansion devices for organic rankine cycle (orc) using in low temperature heat recovery: A review. *Energy Conversion and Management*, 199:111944.

This book contains the compilation of works contributed to the *7th International Seminar on Organic Rankine Cycle Power Systems* (ORC 2023), held in Seville between the 4th and 6th of September 2023. The event was hosted by Universidad de Sevilla on behalf of the Knowledge Centre on Organic Rankine Cycle Technology (KCORC), incorporated in The Netherlands.

The ORC conference, organized biennially, stems as the only conference that is specific to ORC technology, therefore gathering a diverse community whose affiliation spans across all the interested stakeholders, not only in this particular technology but also and in a broader context, in the energy transition. Original equipment manufacturers, professional associations, end-users, investors, policy makers, academics, scientists feel at home at ORC 2023.

The almost 100 proceedings in this book cover a wide variety of topics, from fundamentals to system integration through component design, accounting for thermodynamic performance as well as component design. In addition to this, and as a new track in 2023, works on heat pump technology were also accepted in order to raise awareness of the strong ties between both technologies, specifically in energy storage applications.

This book provides an excellent overview of the current maturity of power systems based on Organic Rankine Cycle technology for applications as diverse as geothermal and waste heat recovery in industry or downstream of other prime movers (e.g., marine applications). It is also an excellent source of information to understand the current challenges faced by the technology, stemming from a very competitive market and increasingly stringent environmental regulations.

The organizers of ORC 2023 hope that the reader finds this work as exciting as the attendees to the conference and, maybe, make the decision to join the 8th edition to the conference in 2025.

KCORC
KNOWLEDGE CENTER
ORGANIC RANKINE CYCLE

eUS EDITORIAL
UNIVERSIDAD DE SEVILLA